Imaging of a vibrating object by Sideband Digital Holography

Michel Gross, Franck Laloë, Michael Atlan, Jean Hare

Imaging of a vibrating object by Sideband Digital Holography

M. Gross[1], F. Laloë[1], M. Atlan[2] and J. Hare[1]

[1] *Laboratoire Kastler Brossel – UMR 8552 École Normale Supérieure, UPMC, CNRS 24 rue Lhomond ; 75231 Paris Cedex 05 ; France*

[2] *Département de Biologie Cellulaire — Institut Jacques Monod, CNRS UMR 7592, Univ. Paris 6 and 7 — 2 Place Jussieu ; 75251 Paris Cedex 05; France*

gross@lkb.ens.fr

Abstract: We propose a new method for imaging vibrating objects. The frequency sidebands on the light scattered by the object, shifted by n times the vibration frequency, are selectively detected by heterodyne holography, and images of the object are calculated for different sideband orders n. Orders up to $n = 120$ have been observed, allowing the detection of amplitudes of oscillation that are much larger than the optical wavelength. We check that the signal on the sideband n is proportional to $|J_n(z)|^2$, where z is the modulation amplitude for the phase, and J_n a Bessel function of the first kind. Using the data obtained for each value of n, we reconstruct the shape of vibration the object with accuracy.

OCIS codes: 090.1760,200.4880,040.2840,290.3700,290.7050,170.3010,170.6480

References and links

1. R. Powell and K. Stetson, "Interferometric vibration analysis by wavefront reconstruction," J. Opt. Soc. Am. **55**, 1593–1598 (1965).
2. P. Picart, J. Leval, D. Mounier, and S. Gougeon, "Time-averaged digital holography," Opt. Lett. **28**, 1900–1902 (2003).
3. F. Zhang, J. Valera, I. Yamaguchi, M. Yokota, and G. Mills, "Vibration Analysis by Phase Shifting Digital Holography," Opt. Rev. **11**, 297–299 (2004).
4. A. Asundi and V. Singh, "Time-averaged in-line digital holographic interferometry for vibration analysis," Appl. Opt. **45**(11), 2391–2395 (2006).
5. V. Singh, J. Miao, Z. Wang, G. Hegde, and A. Asundi, "Dynamic characterization of MEMS diaphragm using time averaged in-line digital holography," Opt. Commun. **280**, 285–290 (2007).
6. N. Demoli and D. Vukicevic, "Detection of hidden stationary deformations of vibrating surfaces by use of time-averaged digital holographic interferometry," Opt. Lett. **29**, 2423–2425 (2004).
7. N. Demoli, "Real-time monitoring of vibration fringe patterns by optical reconstruction of digital holograms: mode beating detection," œ**14**, 2117–2122 (2006).
8. F. LeClerc, L. Collot, and M. Gross, "Numerical Heterodyne Holography Using 2D Photo-Detector Arrays," Opt. Lett. **25**, 716 (2000).
9. F. Pinard, B. Laine, and H. Vach, "Musical quality assessment of clarinet reeds using optical holography," J. Acoust. Soc. Am. **113**, 1736 (2003).
10. M. Facchinetti, X. Boutillon, and A. Constantinescu, "Numerical and experimental modal analysis of the reed and pipe of a clarinet," J. Acoust. Soc. Am. **113**, 2874–2883 (2003).
11. I. Yamaguchi and T. Zhang, "Phase-Shifting digital holography," Opt. Lett. **18**(1), 31 (1997).
12. M. Atlan, M. Gross, and E. Absil, "Accurate phase-shifting digital interferometry," Opt. Lett. **32**, 1456–1458 (2007).
13. E. Cuche, P. Marquet, and C. Depeursinge, "Spatial filtering for zero-order and twin-image elimination in digital off-axis holography," Appl. Opt. **39**, 4070–4075 (2000).
14. M. Gross and M. Atlan, "Digital holography with ultimate sensitivity," Opt. Lett. **32**, 909–911 (2007).

15. M. Gross, M. Atlan, and E. Absil, "Noise and aliases in off-axis and phase-shifting holography," Appl. Opt. **47**, 1757–1766 (2008).
16. U. Schnars and W. Jüptner, "Direct recording of holograms by a CCD target and numerical reconstruction," Appl. Opt. **33**, 179–181 (1994).

Holographic imaging is based on interferences between a signal optical field and a reference beam; it provides an accurate method to image the vibration of various objects. In their pioneering work [1] Powell and Stetson have shown that the *time-averaged* hologram of an harmonically vibrating object involves the Bessel function $J_0(z)$, where z is the phase modulation amplitude. In the backscattering geometry considered below, $z = 4\pi A/\lambda$ where A is the mechanical amplitude of vibration and λ the optical wavelength. Image reconstruction then provides a direct mapping of the amplitude A, at various points of the object, in the form of dark fringes appearing at points where $J_0(z)$ is nearly zero.

Picard et al. [2] have simplified the processing of the data by performing Time Averaged Digital Holography (TADH) with a CCD camera, yielding numerous recent developments [3, 4, 5, 6, 7].

Nevertheless, with TADH, the quantitative measurement of vibration amplitudes remains limited to situations where fringes can be unambiguously counted. Therefore, the amplitudes of vibration must remain relatively small; when they are too large, it becomes difficult to count many narrow fringes, and even impossible when they are smaller than the optical resolution of the holographic reconstruction.

To overcome this problem, we propose a new holographic technique, which we call "Sideband Digital Holography" (SDH). It is based on heterodyne digital holography [8], where both the reference and the illumination beams are frequency-shifted, where a given frequency sideband of the signal backscattered by the object is isolated by a proper detuning of one of the laser beams and heterodyne detection on a CCD camera. As a demonstration, inspired by the work described in Refs. [9, 10] we perform an experiment where the vibrating object is the reed of a clarinet; in addition to the intrinsic interest of such an object, with its possible musical

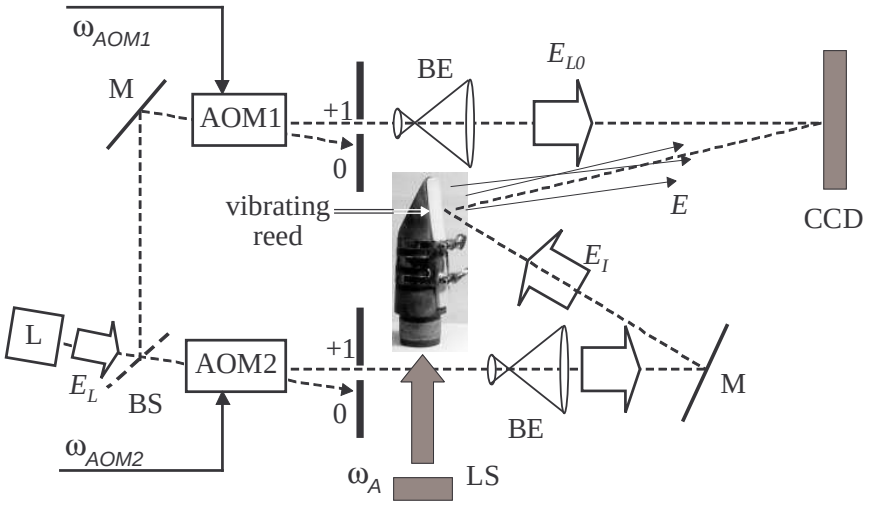

Fig. 1. Setup. L: main laser; AOM1,2 : acousto-optic modulators; M: mirror; BS: beam splitter; BE: beam expander; CCD: CCD camera; LS: loud-speaker exciting the reed.

implications, a reed provides a test system that is particularly well adapted to our purposes, with typical vibration amplitudes of the order of 0.1 mm. We will see that, even with smaller amplitudes, there is no special difficulty in obtaining holographic images corresponding to the n^{th} sideband with n up to 100, or more.

The experimental setup is schematically shown in Fig. 1. A laser beam, with wavelength $\lambda \simeq 650$ nm (angular frequency ω_L) is split into a local oscillator beam (E_{LO}) and an illumination beam (E_I); their angular frequencies ω_{LO} and ω_I are freely tuned by using two acousto-optic modulators (Bragg cells with a selection of the first order diffraction beam) AOM1 and AOM2: $\omega_{LO} = \omega_L + \omega_{\text{AOM1}}$ and $\omega_I = \omega_L + \omega_{\text{AOM2}}$ where $\omega_{\text{AOM1,2}}/2\pi \simeq 80$ MHz. The clarinet reed is attached to a clarinet mouthpiece and, as in usual playing conditions, its vibration is driven by a sound wave propagating inside the mouthpiece; in our experiment this wave is created by a loudspeaker excited at frequency ω_A (no attempt has been made to reproduce the mechanical effect of the lip of the player). The excitation frequency is adjusted to be resonant with the first flexion mode (2143 Hz) of the reed.

Because of the vibration, the phase of the field E backscattered by the reed is phase modulated at frequency ω_A. This field E can thus be expanded into carrier (E_0) and sideband components (E_n) as:

$$E(t) = \mathscr{E} e^{j\omega_I t} e^{jz\sin(\omega_A t)} = \sum_{n=-\infty}^{\infty} E_n(t) \qquad \text{with} \qquad E_n(t) = \mathscr{E} J_n(z) e^{j\omega_L t} e^{j(\omega_{AOM2} + n\omega_A)t} \quad (1)$$

where $\mathscr{E}$ is the complex field of the object without modulation, z is the phase modulation amplitude, $j^2 = -1$, and J_n is the n-th order Bessel function of the first kind (with $J_{-n}(z) = (-1)^n J_n(z)$ for integer n and real z).

To selectively detect the n^{th} sideband we use 4 phase shifting holography [11] by adjusting the frequency ω_{AOM1} to fulfil the condition:

$$\omega_{\text{AOM2}} - \omega_{\text{AOM1}} - n\,\omega_A = \omega_{\text{CCD}}/4 \quad (2)$$

where ω_{CCD} is the CCD camera frame frequency and n is a (positive or negative) integer; the phase of the modulated signal is then shifted by 90° from one CCD image to the next, with a nearly perfect accuracy, since the phase shift is related to frequency differences of beating signals [12]. The sideband complex hologram signal H_n provided by each pixel of the camera, proportional to the local sideband complex field, is obtained by 4-phase demodulation:

$$H_n = (I_0 - I_2) + j(I_1 - I_3)\ , \quad (3)$$

where $I_0, \cdots I_3$ are 4 consecutive intensity images digitally recorded by the CCD camera (Pike: Allied vision Technology Inc, 12 bits, $\omega_{\text{CCD}}/2\pi = 10$ Hz, exposure time 100 ms, 1340×1024 pixels). The LO beam is slightly angularly shifted ($\sim 1^\circ$) with respect to the beam originating from the reed; in this way, the zero order and twin-image aliases [13] can be suppressed and an ultimate detection sensitivity can be reached [14, 15].

From the complex holograms, the images of the reed are reconstructed by the standard convolution method [16]. To simplify the Fourier transform calculation, the 1340×1024 pixels data are truncated to 1024×1024. Because of the angular shift, the image of the reed lies in the upper side of the reconstruction grid. In Fig. 2, for pixels ranging from 0 to 511 along the x axis and 0 to 1023 on the y axis, we show the reconstructed images for different sideband orders n; only the square modulus of the complex signal is retained (the phase coming from $\mathscr{E}$ is ignored), so that we obtain intensity images, proportional to $|E_n|^2$ for each different sideband.

Fig. 2(a) is obtained at the unshifted carrier frequency ($n = 0$). The left side of the reed is attached to the mouthpiece, and the amplitude of vibration is larger at the tip of the reed

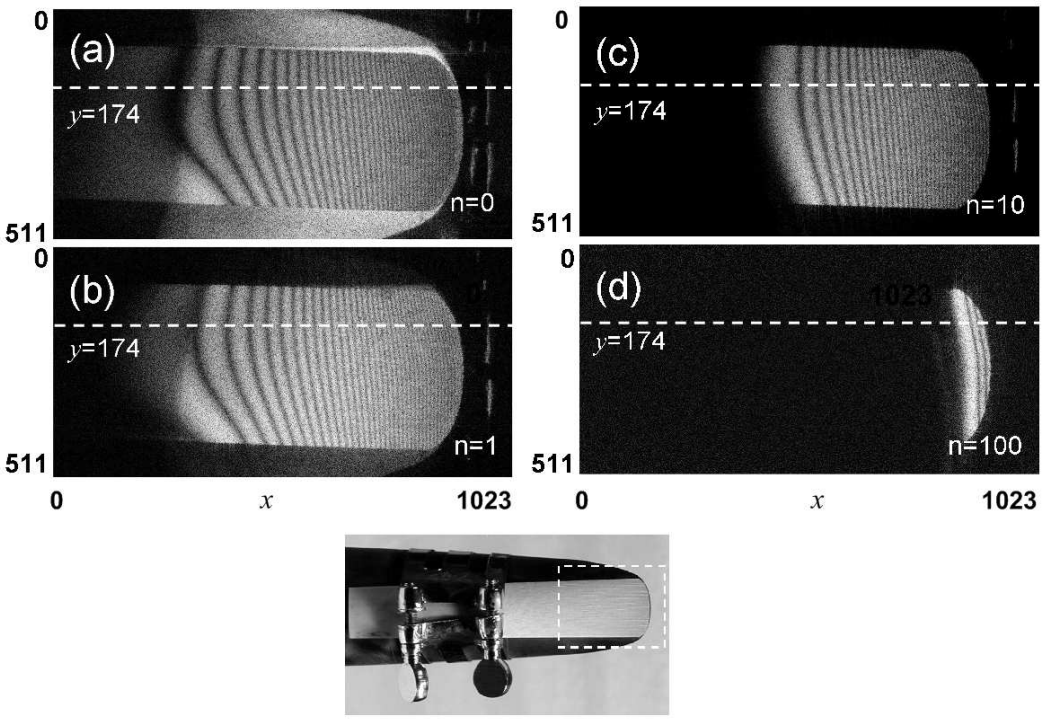

Fig. 2. Reconstructed holographic images of a clarinet reed vibrating at frequency $\omega_A/2\pi =$ 2143 Hz. Fig. (a) shows the carrier image obtained for $n = 0$. Fig. (b), (c) and (d) show the frequency sideband images respectively for $n = 1$, $n = 10$, and $n = 100$. A logarithmic grey scale has been used. Fig. (e) is a photographic image of the reed mounted on its mouthpiece, with the vibrating part (the tip) on the right; the vibration is perpendicular to the plane of the figure. The dashed white rectangle shows the zone covered by the reconstructed holographic images.

on the right side; in this region the fringes become closer and closer and difficult to count. The mouthpiece is also visible, but without fringes since it does not vibrate. Similar images of clarinet reeds have been obtained by TADH in Refs. [9, 10], with more conventional techniques and lower image quality. Figs. 2(b,c,d) show images obtained for three sideband frequencies. As expected, the non-vibrating mouthpiece is no longer visible. Fig. 2(b) shows the $n = 1$ sideband image, with J_1 fringes that are slightly shifted with respect to those of J_0. In Figs. 2(d,e), the sideband orders are larger, respectively $n = 10$ (d) and $n = 100$ (e). The left side region of the image remains dark because, in this region, the vibration amplitude is not sufficient to generate these sidebands, $J_n(z)$ being evanescent for $z < n$.

In order to make a quantitative analysis of the data, we have performed cuts of the reconstructed images signal $|E_n(x,y|^2$ obtained for different sideband orders n along the horizontal line $y = 174$ (this value has been chosen because it corresponds to a region where the fringes are orthogonal to the y axis). To reduce the effect of speckle fluctuations, the intensity signal $|E_n(x,y = 174)|^2$ has been averaged over 20 pixels in the y direction ($y = 164 \ldots 184$). Moreover, since the illumination of the reed is not uniform, we have normalized the sideband signal by the reconstructed image intensity $|E|^2$ obtained at the carrier frequency ($n = 0$) without mechanical excitation of the reed (loud-speaker off). The normalized signals $|E_n|^2/|E|^2$ along the cut are shown in Fig. 3 for $n = 0$ (a), $n = 20$ (b) and $n = 60$ (c).

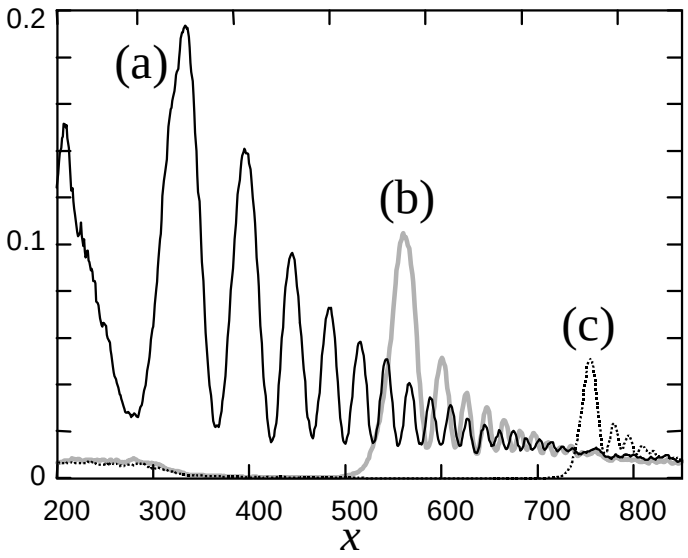

Fig. 3. Cuts along the $y = 174$ line showing the normalized signal $|E_n(x)|^2/|E(x)|^2$ for sideband orders $n = 0$ (a), $n = 20$ (b) and $n = 60$ (c). The horizontal axis is the pixel index along x.

Fig. 3 (a) shows the contribution of the carrier frequency image ($n = 0$), equivalent to standard TADH. The fringes correspond to the variations of $|J_0(z)|^2$, but the horizontal scale x is not merely proportional to z, since z does not increase linearly with x. As expected, the maximal intensity of successive anti-nodes decreases with increasing x (and z) ; above $x = 700$, the fringes are no longer visible. Note that the first fringe ($x \sim 200$) is lower than expected; the reason for this is that, for $x < 300$, the illumination intensity is very low resulting in an inaccurate normalization. Fig. 3 (b) shows the contribution of $n = 20$, i.e. fringes corresponding to $|J_{20}(z)|^2$. The first fringe is located near $x \simeq 560$, corresponding to $z \simeq 20$; it can easily be distinguished from the others since it is higher and broader. This illustrates how sideband holography can provide a reference fringe corresponding to a non-zero modulation amplitude, which is useful for removing ambiguity in fringe counting. In fact, for this particular experiment, counting TADH fringes would probably still be possible, since we study the first reed flexural mode characterized by an amplitude that is monotonous in x. For higher order modes, the counting would be more difficult. Fig. 3 (c) corresponds to $n = 60$, i.e. fringes given by $|J_{60}(z)|^2$. The first fringe ($x \simeq 755$) can easily be distinguished; altogether, about 3 fringes can be observed. The first fringe provides a marker for the region $z \simeq 60$. Note that in this region fringes are no longer visible in curve (a), because they are too narrow; in other words, TADH would no longer be effective. This is a clear illustration of how sideband holography extends the fringe visibility to otherwise unreachable vibrating regions of the reed.

Fig. 4 makes use of the signal obtained for n = 0,1,5,10,... 100. For each n value, a cut along the $y = 174$ line has been extracted out of the reconstructed image. The x locations of the successive minima of the normalized signal $|E_n(x)|^2/|E|^2$ have been noted down. In the figure, they are plotted against the zeros of the corresponding $|J_n(z)|^2$ expected signal. To illustrate the way the points are obtained, we show the expected signal $|J_5(z)|^2$ on the left side of the figure, and the measured normalized signal $|E_5(x,174)|^2/|E(x,174)|^2$ on the bottom side. For all observed sideband order n ranging from 0 to 100, all the points displayed on Fig. 4 fall on a single curve: this very good consistency of the overlapping data demonstrates the validity of the expansions

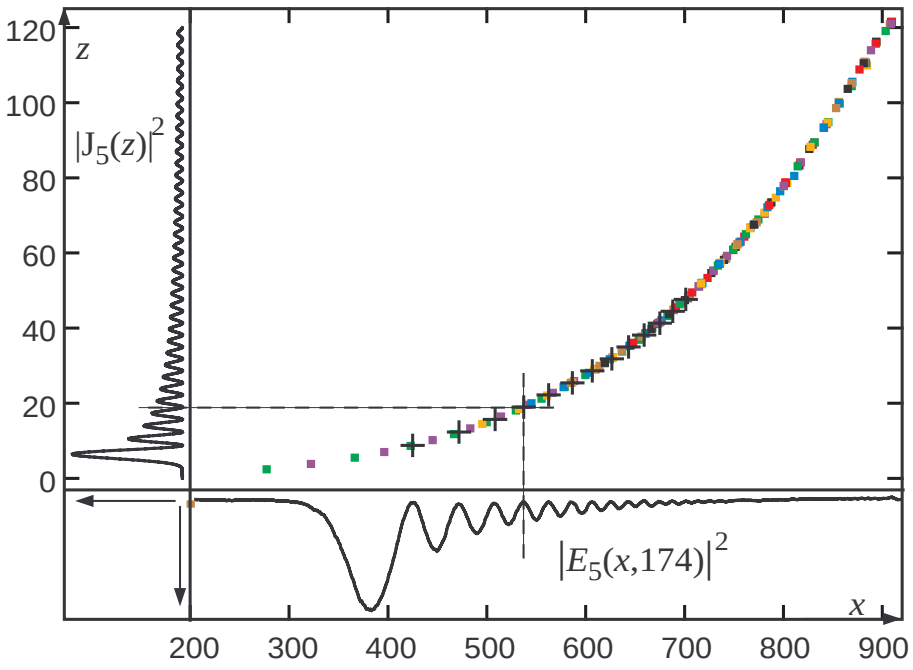

Fig. 4. Variations of z (which is proportional to the amplitude of vibration) as a function of x, expressed in pixel rank (100 pixels correspond to 3.68 mm.). The points are obtained from the minima of the measured signal $|E_n(x,174)|^2/|E(x,174)|^2$ (x axis) and of the corresponding expected signal $|J_n(z)|^2$. A different color is used to display the points obtained for different harmonic order n.

Eq. 1 for any observed sideband order n. The curve exhibits the modulation/vibration amplitude z as function of the location x and hence provides a direct visualization of the shape of the reed at maximal elongation, from the left part clamped on the mouthpiece to the tip on the right. In the present case, the maximum amplitude is $z \simeq 120$ radians, corresponding to $A \simeq 6.2\ \mu$m. To our knowledge, such a quantitative x–z law has not been experimentally demonstrated, even in the TADH case $n = 0$.

To conclude, recording separately different sideband Fourier components of the light backscattered by a vibrating object gives access to a large amount of additional information; this can be used to remove ambiguities and inaccuracies in measurements of large modulation amplitude. Using large sideband order n actually makes the calibration of the vibration amplitude z straightforward: the first fringe of a high order image can be used as a marker, since it is easy to locate since it corresponds to a fast transition from zero signal; moreover, it is brighter and broader. Performing sideband holography with many sideband orders, as illustrated in Fig. 4, gives a direct access to the shape of the vibration amplitude and its position dependence. Sideband digital holography therefore really opens up new possibilities in holography.

The authors acknowledge the French National Research Agency (ANR) and the “Centre de compétence NanoSciences Île de France” (C’nano IdF) for their support.